Application of EDTA modified Fe_3O_4/Sawdust Carbon nanocomposites to ameliorate Methylene Blue and Brilliant Green dye laden water

Navish Kataria[a], V. K. Garg[a,b*]

[a]*Department of Environmental Science and Engineering, Guru Jambheshwar University of Science and Technology Hisar-125001, India*

[b]*Centre for Environmental Sciences and Technology, Central University of Punjab, Bathinda 151001, Punjab, India.*

Corresponding author: Phone +91-9812058109; E-mail - vinodkgarg@yahoo.com

Abstract:

This work explored the potential of magnetic sawdust carbon nanocomposites for cationic dyes removal from aqueous medium. EDTA modified magnetic sawdust carbon nanocomposites (EDTA@Fe_3O_4/SC ncs) were prepared by biogenic green reduction and precipitation approach. The surface properties, structure and composition of nanocomposites were analyzed by HRTEM, FESEM, XRD, EDX, BET, FTIR etc. The Fe_3O_4 nanoparticles were 10-20 nm in diameters and having 14m^2/g surface area. Removal efficiency of Methylene blue (MB) and Brilliant green (BG) from aqueous medium was studied in batch mode experiments. The maximum removal was observed at neutral pH 7.0 with in 30 min. Adsorption capacity of EDTA@Fe_3O_4/SC for MB and BG dyes was 227.3 mg/g and 285.7 mg/g, respectively. Dye adsorption behaviour was well explained by Freundlich model. The rate of cationic dye adsorption was explained by pseudo-second order model. The value of thermodynamic parameters confirmed the adsorption process is spontaneous and favourable. Desorption and reusable efficiency of nanocomposites was also evaluated.

Graphical abstract:

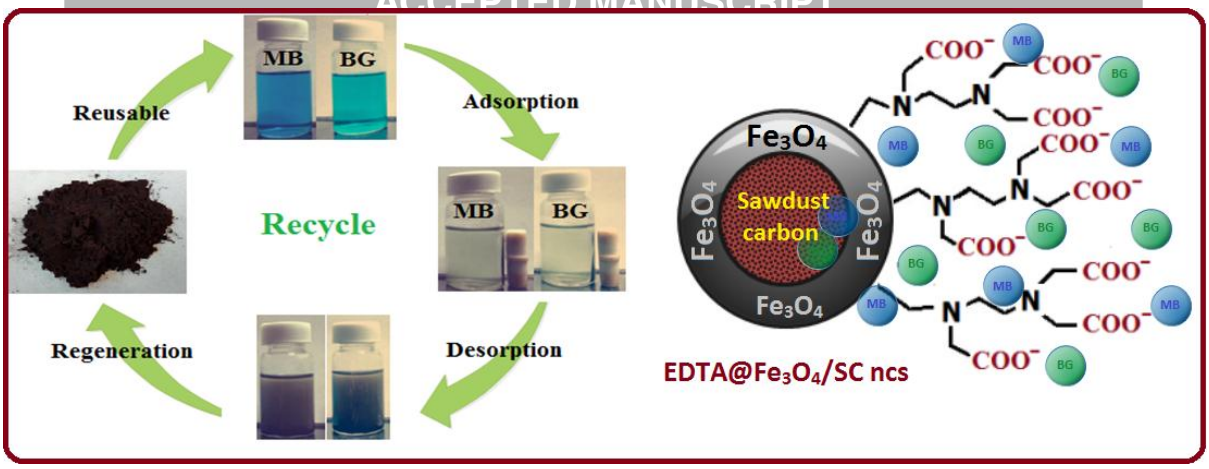

Keywords: Nanocomposites, Green synthesis, Cationic dyes, Isotherms modelling, Regeneration, Adsorption

Introduction:

The discharge of unutilized dyes from industries, viz., paper and pulp, printing, textiles, cosmetics, leather, food processing etc. becomes a serious concern in relation to water pollution (Liu et al., 2012). Currently, more than 100,000 commercial dyes with approximately 700,000 tons of dyestuff annually are produced by industries worldwide. Dye burdened wastewater are toxic, hazardous and carcinogenic in nature due to their complex chemical structure and non-biodegradable nature (Rafatullah et al., 2010; Mittal et al., 2018). Dye contaminated wastewater interrupts the normal aquatic life by decreasing visibility and photosynthetic ability of hydrophytes, increasing biochemical oxygen demand (Zaharia et al., 2009). Methylene blue (MB) dye is a cationic dye with aromatic structure. It is commonly applied to dyeing wool, cotton and silk, colouring paper, food processing, cosmetic products and in research laboratories (Wang et al., 2014; Saini et al., 2018; Makhado et al., 2018). Exposure to MB dye may cause skin and eyes irritation, vomiting, nausea, jaundice, increases heartbeat, methemoglobinemia (decreased oxygen level in blood) (Ai et al., 2011; Gurses et al., 2014; Gusmão et al., 2013; Makhado et al., 2018). Brilliant green (BG) dye is also cationic in nature and having triphenyl nitrogen structure. It is used in biological staining, veterinary drugs, dermatological agents, as an additive to poultry feed to control the multiplication of parasites and fungus, dying textiles products and colour printers inks

(Taneja et al., 2018; Sancheti et al., 2018). It may cause several health problems such as irritation in gastrointestinal tract and respiratory tract, skin and eye irritation with flushing and pain, diarrhoea, coughing, shortness of breath, vomiting, nausea etc. (Nandi et al., 2009; Ghaedi et al., 2015; Makhado et al., 2018a). Cationic dyes are considered more toxic and hazardous as compared to anionic dyes, because their positively charged molecules comfortably bind with negatively charged sites of cell wall. Therefore, cationic dyes' sequestration is important from wastewaters before releasing them in aquatic stream (Pandey, 2017; Mittal et al., 2018).

Several methods including photo-catalytic degradation, advanced oxidation process, ozonation, filtration, coagulation, bioremediation, adsorption, reverse osmosis etc. have been adopted for the treatment of dye laden wastewater (Lin et al., 2016). Each of above techniques has its own benefits and drawbacks. Among these techniques, adsorption is widely used technique for dye decontamination. Adsorption of a dye largely depends on the properties of the adsorbent (Pandey and Ramontja, 2016; Pandey, 2017; Makhado et al., 2018a).

Recent progress in nanotechnology has created attention of scientific community to develop magnetic, low cost and economically viable nanoadsorbents for water treatment. Various nanoadsorbents including graphene (Liu et al., 2012), nanocrystalline cellulose (He et al., 2013), carbon nanotube (Gupta et al., 2013), Gum ghatti/Fe_3O_4 magnetic nanocomposites (Mittal et al., 2014), TiO_2/Cashew nut shell AC (Ragupathy et al., 2015), Gum xanthan/Fe_3O_4 based nanocomposites (Mittal et al., 2016), Gum ghatti/TiO_2 nanoparticles-based hydrogel nanocomposite (Mittal and Ray, 2016), NiS/Ni_3S_4 incorporated polyacrylamide grafted gum karaya bionanocomposite hydrogel (Kumar et al., 2016), ZnO nanoparticles (Kataria and Garg, 2017), ZnO-Activated Carbon (Saini et al., 2017), SiO_2/Fe_2O_3 (Joshi et al., 2018) etc. have been reported by researchers for dye adsorption from aqueous solution. However, these adsorbents are usually problematic or difficult to separate from medium because conventional centrifugation and filtration techniques are laborious and costly. The application of magnetic nanoadsorbent and its magnetic properties are efficient to overcome the problem of separation (Mittal et al., 2014; Ahmed and Ahmaruzzaman, 2015). Hence magnetic nanoadsorbents may be a promising alternate to conventional adsorbents because of their magnetic nature, easiness to separate from solution, large surface area, high dye removal efficiency etc. (Duman et al., 2016, Kataria and Garg, 2018a). Several authors have reported

modification or functionalization of nanomaterials by various chemical compounds and organic acids to enhance adsorption efficiency (Makhado et al., 2018a).

In this work, the magnetic (Fe_3O_4) nanoparticles loaded sawdust and EDTA modified magnetic sawdust carbon (EDTA@Fe_3O_4/SC) nanocomposites has been synthesized and utilized for cationic dye removal.

2. Experimental Description:

2.1. Material and Reagents:

The chemicals used in this work were AR grade reagents. Poplar sawdust (*Populus*) was collected from a saw mill in city of Jagadhri, Haryana, India. Ferric nitrate [Fe $(NO_3)_3.9H_2O$], EDTA disodium salt [$C_{10}H_{14}N_2Na_2O_8$] and Liquor ammonia (25%) were procured from Qualigen Fine Chemicals Pvt., Ltd, Mumbai. Methylene blue (MB) dye [Mol. formula- $C_{16}H_{18}ClN_3S$, C.I no.- 52015, M.wt.- 319.9g/mol, λ_{max} - 664nm] and Brilliant Green (BG) dye [Mol. formula- $C_{27}H_{34}N_2O_4S$, C.I no.- 42040, M.wt.- 482.6 g/mol, λ_{max} - 625nm], sodium hydroxide (NaOH) pellets, Hydrochloric acid (HCl), ethanol and methanol were purchased from SD fine-chem Ltd, Mumbai. All stock and working solutions were prepared using double distilled water.

2.2. Preparation of EDTA@Fe_3O_4/SC nanocomposites:

EDTA modified Fe_3O_4 nanoparticles loaded sawdust carbon nanocomposites were synthesized by low cost biogenic green synthesis process as reported earlier (Kataria and Garg 2018a). In this method, sawdust was washed with double distilled water followed by oven drying, grinding and sieving with 250 mesh sieve. 3.0 g sieved sawdust was mixed into 100 mL double distilled water and added 4.0 g $Fe(NO_3)_3$ as source of iron into solution under strong stirring up to 60 min at 90 ˚C. The reduction of Fe^{3+} to Fe^{2+} took place. Liquor ammonia (25%) was added in solution under sonication upto pH 10 that yielded black colour Fe_3O_4 nanoparticles loaded sawdust nanocomposites. These were separated from solution by magnet and surface impurities were removed washing with double distilled water. The material was carbonized in vacuum furnace at 180 ˚C overnight. Final product (Fe_3O_4/Sawdust Carbon nanocomposites) was stored in plastic container to utilize in further experiments.

To prepare EDTA@Fe_3O_4/SC ncs, 1.0g Fe_3O_4/SC ncs were added to 100 mL solution of EDTA-disodium salt (4.0 g) and sonicated for 30 min. After sonication, the mixture was kept in orbital shaker for 12 h at 150 rpm. The synthesized EDTA@Fe_3O_4/SC ncs were extrated using magnet and washed several times with double distilled water. These nanocomposites were dried and stored for characterization and adsorption studies. Schematic description of EDTA@Fe_3O_4/SC ncs synthesis is given in Fig. 1.

The synthesized nanocomposites was characterized using XRD (Rigaku Miniflex-II diffractometer, USA, Canada), FTIR spectrophotometer (Shimadzu IR AFFINITY-I, Japan), and FESEM Carl Zeiss, (Merlin Compact 6073, Germany). Dye content in the solution was quantified by UV- Visible spectrophotometer (UV–VIS 3000^+ LABINDIA, India). TEM images and SAED patterns were acquired using FEI Tecnai G^2 20 TWIN microscope (USA) operating at 200 kV. BET analyzer (Quantachrome Nova 2000e) was used to evaluate the Surface area and porosity. Salt addition method was used to determine the pH at point of zero charge (pHpzc).

2.3. Adsorption experiments:

Adsorption of dyes onto the EDTA@Fe_3O_4/SC ncs was explored in batch mode. The stock solution of 500 mg/L concentration of each dye was prepared and diluted further to prepare working solution of desired concentration. pH of solutions were adjusted using NaOH (0.1M) or HCl (0.1M) solutions. All dye adsorption studies were carried out in 250 mL Erlenmeyer flasks employing 50 mL dye solution of pre-determined dye concentration and adsorbent dose. The dye and adsorbent mixture was shaken in thermostatic orbital shaker at 180 rpm under dark conditions. After adsorption equilibrium, nanocomposites were separated from dye solution using magnet and residual MB and BG concentration in solution was determined using UV-VIS Spectrophotometer. The influence of salinity onto dye adsorption was evaluated at different NaCl concentrations (0.05 to 0.8M). The adsorption efficiency for dyes was also determined in real water sample. The dye removal (%) and adsorption capacity (mg/g) of the adsorbent was wuantified by using the equations (1) and (2), respectively.

$$\text{Dye removal } (\%) = \frac{(C_o - C_e)}{C_o} \times 100 \quad (1)$$

$$\text{Adsorption capacity } (q_e) = \frac{(C_o - C_e)\, V}{m} \quad (2)$$

Where C_o (mg/L) is the initial MB and BG concentration in solution, C_e (mg/L) is the equilibrium MB and BG concentration in solution, q_e (mg/g) is the amount of MB and BG adsorbed onto adsorbent at equilibrium, m (g) is the mass of the EDTA@Fe_3O_4/SC ncs and V (L) is the volume of cationic dye solution used.

2.4. Adsorption modelling:

Isotherms, kinetics and thermodynamic studies were performed to assess the adsorption behaviour and rate-mechanism of cationic dye molecules onto adsorbent. Langmuir (Langmuir, 1916), Freundlich (Freundlich,1906), Temkin (Temkin and Pyzhev, 1940) and Dubinin- Radushkevich (Dubinin and Radushkevich, 1947) isotherms were applied to experimental data to explore the cationic dye adsorption.

A linear form of Langmuir model is represented as equation (3).

$$\frac{C_e}{q_e} = \frac{1}{q_{max} b} + \frac{C_e}{q_{max}} \quad (3)$$

Where, C_e (mg/L) and q_e (mg/g) is described above, q_{max} (mg/g) is the Langmuir maximum adsorption capacity, b (L/mg) is the Langmuir constant. The value of q_{max} and b is calculated from linear plot between *Ce/qe* vs *Ce*. The essential features of the Langmuir isotherm can be explained by the equilibrium parameter R_L, represented as equation (4).

$$R_L = \frac{1}{1 + bC_O} \quad (4)$$

Where, R_L is dimensionless constant and its value indicate that the adsorption isotherm is to be either favourable if $0< R_L <1$, unfavourable if $R_L >1$, irreversible if $R_L=0$ or linear if $R_L=1$. Freundlich isotherm model is written as equation (5)

$$log q_e = log K_f + \frac{1}{n} log C_e \quad (5)$$

Where, K_f (mg/g $(L/mg)^{1/n}$) is Freundlich constant and 1/*n* is the heterogeneity factor indicate the intensity of adsorption. K_f and n is quantified using linear plotting between *log* q_e vs *log* C_e,. It is stated that the value of 1/*n* should be lie in between 0 to 1 for favourable adsorption and it indicates the intensity of adsorption on heterogeneous surface. The value of 1/n closer to zero shows highly heterogeneous surface, if 1/n < 1, designates adsorption through

chemisorption process and if 1/n > 1, denotes cooperative adsorption (Foo and Hameed, 2010).

Temkin isotherm model is represented as equation (6).

$$q_e = BlnK_T + BlnC_e \quad (6)$$

Where B = *RT/b*, *b* (J/mol) is the Temkin constant related to heat of adsorption and K_T (L/g) is equilibrium binding constant. K_T and B were quantified using plots of q_e vs *ln* C_e.

Dubinin- Radushkevich isotherm model is represented as equation (7). ε is Polanyi potential and E (KJ/mol) is the mean adsorption energy and calculated from equation (8) and (9), respectively.

$$lnq_e = lnQ_s - K_D\,\varepsilon^2 \quad (7)$$

$$\varepsilon = RT\ln(1 + 1/C_e) \quad (8)$$

$$E = 1/\sqrt{2K_D} \quad (9)$$

Where Qs (mg/g) is the maximum amount of cationic dye adsorption and K_D (mol^2/KJ^2) is the mean adsorption energy. The value of Qs and K_D is calculated from linear plotting between *ln* q_e vs *ε*.

Kinetics of cationic dyes adsorption was determined by applying pseudo-first order (Langergren, 1898), pseudo-second order (Ho and Mckay, 1999) and intraparticle diffusion (Weber and Morris, 1963) equations.

A linear form of pseudo-first order is written as equation (10).

$$\log(q_e - q_t) = log\ q_e - \left(\frac{k_1}{2.303}\right)t \quad (10)$$

Where, q_t (mg/g) is the amount of MB and BG dye adsorption at time *t* and k_1 (min^{-1}) is the pseudo –first order rate constant. The value k_1 and q_e was calculated from linear plot between *log* $(q_e - q_t)$ vs *t*. Pseudo-second order model linear from is written as equation (11).

$$\frac{t}{q_t} = \frac{1}{k_2\,q_e^2} + \frac{t}{q_e} \quad (11)$$

Where k_2 (g/mg min) is the pseudo-second oder rate constant. The value of k_2 and q_e (cal) was quantified using linear graph plotting between t/q_t vs t. Intra-particle diffusion model linear form is written as equation (12).

$$q_t = k_{id}\, t^{1/2} + C \tag{12}$$

Where, k_{id} (mg $g^{-1}min^{-1/2}$) and C (mg/g) are the intra-particle diffusion rate constants and intercept related to thickness of boundary layer, respectively. Here, k_{id} and C values were calculated using linear plots between q_t vs $t^{1/2}$.

Thermodynamics of cationic dyes adsorption was evaluated by change in Gibb's free energy (ΔG^{o}), entropy (ΔS^{o}) and enthalpy (ΔH^{o}). These thermodynamic parameters were calculated using Van't Hoff equation (Van't Hoff, 1884; Crini and Badot, 2008) (13) and (14).

$$\Delta G^0 = -RTlnK_d = \Delta H^0 - T\Delta S^0 \tag{13}$$

$$lnK_d = \frac{\Delta H^0}{RT} - \frac{\Delta S^0}{R} \tag{14}$$

Where, R is gas constant (8.314 J mol^{-1} K^{-1}), T is the temperature (K) and K_d is the equilibrium constant and represented as (15).

$$K_d = \frac{C_a}{C_e} \tag{15}$$

Where, C_a (mg/L) is the concentration of MB and BG onto adsorbent and C_e (mg/L) is the concentration MB and BG in solution at equilibrium The ΔH^{o} and ΔS^{o} were calculated from the slope and intercept respectively obtained from plot between lnk_d vs 1/T.

2.5. Desorption and Reusability

Desorption of MB and BG dye from EDTA@Fe_3O_4/SC ncs was explored using five desorbing solutions. Initially, MB and BG dye (30 mg/L) adsorption from 30 mL dye solution under optimum conditions was allowed on the nanocomposites. After that spent adsorbent was separated from solution by magnet followed by stripping in 30 mL solution of ethanol, methanol, HCl (0.1M), NaOH (0.1M) and distilled water, separately in orbital shaker. The nanocomposites were extracted from solution and concentration of MB and BG dye in supernatant was quantified using UV-VIS Spectrophotometer. The spent nanocomposites were washed and dried for further use. Five cycles of adsorption–desorption were studied.

The reusability of nanocomposites was calculated after each cycle. Desorption percentage was calculated using equation (3):

$$\text{Desorption (\%)} = \frac{\text{Eluted dye concentration } (C_d)}{\text{Initial dye concentration } (C_a)} \times 100 \quad (3)$$

3. Result and Discussion:

3.1 Characterization of synthesized nanocomposites:

XRD of Fe_3O_4/SC and EDTA@ Fe_3O_4/SC ncs is depicted in Fig. 2a. It was studied to clarify the structure and composition of synthesized nanocomposites. The obtained diffraction peak at 2θ = 26.5 with their corresponding plane (002) indicated the presence of sawdust carbon. The XRD diffraction peaks with some noise at 2θ = 29.9 (220), 35.34 (311), 43.04 (400), 57.34 (511) and 62.48 (440) designated the presence of crystalline iron oxide (Fe_3O_4) nanoparticles in nanocomposites (Liu et al., 2015). After chemical modification, similar pattern of XRD was observed which illustrate the no change in nanocomposites.

Fig. 2b, shows the FTIR spectra of EDTA@Fe_3O_4/SC ncs before and after MB and BG dyes adsorption. The broad absorption band in region 3300-3500 cm^{-1} may be due to O-H stretching and bending vibrations of water molecules and O-H group of EDTA. The absorption peak at region 2800- 2900 cm^{-1} attributed to stretching vibration of C-H bond. The sharp peaks at 1724 and 1637 cm^{-1} correspond to C=O and C–O bond which indicated the carboxylic acid group (Liu et al., 2013). Several small peaks in the region 1250-1500 cm^{-1} attributed to C–H, C–N stretching and O–H bending vibration and IR peak at 1037 cm^{-1} attributed to aliphatic C–N stretching vibration. All these absorption peaks indicated the presence of EDTA on the surface of adsorbent. The absorption peaks at 503 and 416 cm^{-1} attributed to Fe–O group of iron oxides. After cationic (MB and BG) dyes adsorption some changes in IR spectra of adsorbent were observed. A decrease in band intensity at region 3300-3500 cm^{-1} indicates that the hydroxyl group of EDTA involved in cationic dyes adsorption (Wang et al., 2014). Two new peaks observed at 2337 cm^{-1} and 634 cm^{-1} attributed to C=N stretching of aromatic tertiary amine and C–H stretching of benzene rings, respectively. It confirmed the existence of MB and BG dye on the surface of adsorbent. Disappearance of absorption peak at 1637 cm^{-1} indicates at COO^- group of adsorbent bind with MB and BG dyes. Increase and shift in peaks at 1200- 1500 cm^{-1} region confirmed the binding of MB and BG dye on the surface functional groups of the adsorbent. These peaks

attribute to (C–H) methyl, (C=C) aromatic ring, $–CH_2$ and $–CH_3$ stretching vibration of MB and BG dyes. These characteristic peaks of FTIR confirmed that the surface functional ($OH^–$ and $COO^–$) group of EDTA was involved in MB and BG dye adsorption.

Fig. 2c encapsulates the FESEM image of synthesized EDTA@Fe_3O_4/SC nanocomposites at 250 kX magnification. The surface morphology and texture showed that spherical shape iron oxide nanoparticles were agglomerated on the sawdust carbon. After EDTA modification iron oxide nanoparticles were distributed on surface, in pore etc of sawdust carbon. Energy Dispersive X-ray spectra and elemental composition of EDTA@Fe_3O_4/SC nanocomposites are given in Fig. 2d. In this spectrum, iron (~ 6.5 keV), carbon (~ 0.3 keV) and oxygen (~ 0.5 keV) energy peaks were observed which indicate the elemental composition of nanocomposites. The wt% of C, O, Fe, elements in nanocomposites was 25.03%, 25.5%, 49.5%, respectively (Fig. 2d). It indicated that the synthesized material is iron oxide sawdust carbon (EDTA@Fe_3O_4/SC) nanocomposite.

The BET surface area, pore size and pore volume distribution of prepared nanocomposites were analysed by BET analyser. Fig. 2e shows the Nitrogen adsorption–desorption isotherms plot and inset BJH pore size distribution plots of EDTA@Fe_3O_4/SC nanocomposites. The BET surface area of EDTA@Fe_3O_4/SC nanocomposites was 14 m^2/g. BJH pore diameters and pore volume was 3.18 nm and 0.086 cc/g. It attributed to the available active sites on the surface of adsorbent that enhance the binding affinity of dye molecules. The adsorption of dye molecules is a surface phenomenon Adsorption of dye molecules depends on surface area, surface functional groups and porosity of adsorbent (Lee et al., 2008). The porous structure (i.e., pore size and pore volume) and surface area contributed in the suitable binding sites for the dye adsorption. The pH at the potential of zero charge (pHpzc) of nanocomposites was determined using plot between ΔpH and pHi as shown in Fig. 2f. The obtained value of pHpzc of Fe_3O_4/SC and EDTA@Fe_3O_4/SC nanocomposites was 4.3 and 6.1, respectively.

Internal crystalline structure and size of synthesized Fe_3O_4/SC and EDTA@Fe_3O_4/SC nanocomposites were interpreted by TEM micrograph and SEAD pattern [Fig. 3(a-f)]. Fig. 3a and 3c depict the spherical and hexagonal shaped Fe_3O_4 nanoparticles agglomerated on sawdust carbon and their particles size varied from 5 nm to 15 nm. After EDTA treatment, these spherical iron oxide nanoparticles were dispersed and distributed on sawdust carbon are shown in Fig. 3b and 3d. The particles size was uniform in the range of 10 to 20 nm. Fig. 3e

and 3f depicts the corresponding selected area electron diffraction (SEAD) pattern of Fe_3O_4/SC and EDTA@Fe_3O_4/SC nanocomposites. In this pattern, the well-defined diffused ring is formed by small white spots which correspond to the polycrystalline iron oxide nanoparticles distributed on amorphous sawdust carbon. Each circular ring formed with white spot correspond to diffraction plane (220), (311), (400) and (440) which assigned for the crystalline Fe_3O_4 as shown in Fig. 3e. After EDTA modification, the white spots dispersed in diffused circular ring assigned for crystalline Fe_3O_4 nanaoparticle with diffraction plane (220), (311), (400), (511) and (440) dispersed in amorphous sawdust carbon (Fig. 3f). The crystalline iron oxide nanoparticle dispersed in pores of sawdust carbon and it may decrease the porosity as well as surface area of adsorbent. High crystallinity of adsorbent decreased to the amorphous and porous character of adsorbent due to decrease in surface area (Jegadeesan et al., 2010; Yu et al., 2015). The crystalline structure has fewer moieties and fewer defects that affect the internal sites of adsorbent at which either chemical or physical interaction of dye molecules occurred. Dye molecules adsorption is associated to surface area, porous structure and surface binding sites. Crystalline structure indirectly decreases the dye adsorption efficiency of adsorbent due shortage of internal pore sites and surface active sites (Yang, et al., 2010). SAED pattern of nanocomposites was also supported by XRD spectra of Fe_3O_4/SC and EDTA@Fe_3O_4/SC nanocomposites.

3.2 Batch mode adsorption experiments:

3.2.1 Effect of pH:

pH is an important parameter for solid/liquid interface that alter the surface properties of adsorbent as well as chemistry of adsorbate. To explore the effect of solution pH onto MB and BG dye adsorption, adsorbate solution pH was varied from 2.0 to 10.0 (Fig. 4a and b). All other experimental parameters, dye concentration: 30 mg/L, adsorbent dose: 0.4 g/L, contact time: 90 min. and temperature: 27 ˚C, were kept constant. The adsorption of MB and BG dye onto EDTA@Fe_3O_4/SC improved from 71.7 to 99.5% and 58.7 to 93.0%, respectively with rise in solution pH from 2.0 to 6.0 (Fig. 4a and b). The pHpzc of EDTA@Fe_3O_4/SC was 6.1. At lower pH (≤ pHpzc), the surface of adsorbent was extremely positively charged ($X–COOH_2^+$) due to excess number of hydrogen ions (H^+), that promoting the electrostatic repulsion between cationic dyes and adsorbent surface (Gusmão et al., 2013; Kataria and Garg, 2017). Therefore, minimum removal was observed. As pH increased upto

pHpzc, the electrostatic attraction between adsorbent surface ($X–COO^-$) and dye molecules increased due to increase in deprotonation of the adsorbent surface that enhanced the MB and BG dye adsorption (Garg et al., 2004). After further increase in pH (≥ pHpzc), not much increase was observed in dye removal. It may be due to infinite number of active sites generated that was enough for dye adsorption or saturation of dye adsorption. Similarly in case of Fe_3O_4/SC, the removal efficiency gradually increased with pH as shown in Fig. 4a and b. The adsorption efficiency of EDTA@Fe_3O_4/SC for MB and BG dye was 99.7% and 96.7%, respectively that is higher than Fe_3O_4/SC. After EDTA modification, the surface of adsorbent was covered with carboxyl and amine group that strongly bind with cationic species via electrostatic and H-H interaction (Liu et al., 2013). The pH for other experiments was optimized at 7.0 for both the dyes.

3.2.2 Effect of MB and BG concentration and contact time:

The role of MB and BG concentration on the adsorption of cationic dye was studied by varying dye concentration from 10 to 100 mg/L and all other parameters remains constant. The removal of MB and BG dyes decreased from 99.7 to 88.3% and 96.0 to 83.5%, respectively with rise in initial dye concentration (Fig. 5a). Similar observation for dye adsorption has been reported by other researchers (Saini et al., 2018; Nandi et al., 2009). At lower dye concentration, the numbers of available energetic binding sites ($X–COO^-$) on the surface of EDTA@Fe_3O_4/SC ncs was higher as compared to adsorbing dye molecules, resulting maximum adsorption. With increase in dye concentration, dye adsorption reduced gradually due to decrease in number of active binding sites as compared to dye molecules and increase the competition between cationic dye molecules adsorption on the surface active sites of adsorbent (Garg et al., 2004; Kataria and Garg, 2017). To effect of contact time on dye adsorption has been studied at three different dye concentrations (10, 50 and 100 mg/L) by varying contacting time from 5 to 90 min (Fig. 5b and c). The maximum amount of MB dye (~ 90%) was removed within initial 10 min. it may be attributed the large number of active sites as carboxyl and amino group on the adsorbent surface that rapidly and strongly bind with MB dye (Fig. 5b). After that slight increment in dye removal was observed with contact time and equilibrium was attained at 60 min due to saturation of active sites with MB dye molecules. In case of BG dye, the removal of BG dye increased with contact time up to 30 min and equilibrium was attained at 90 min (Fig. 5c). Initially, excess numbers of unoccupied active sites were available to BG dye for adsorption which was saturated at equilibrium. At lower dye concentration, the removal of cationic dye is achieved within

minimum initial contact time as compared to high dye concentration (Ahmed and Ahmaruzzaman, 2015).

3.2.3 Effect of adsorbent dose:

The EDTA@Fe_3O_4/SC ncsdose altered from 0.001 to 0.08 g/50 mL to explore its effects on the removal of 50 mg/L MB and BG dyes from aqueous medium. All other experimental parameters kept constant including pH: 6.5, temperature: 27±1˚C, contact time: 120 min. The removal of MB and BG dye increased from 20.4 to 98.7% and 36.7 to 97.3%, respectively with increase in adsorbent dose. Initially, rapid removal of dye was observed with increase in adsorbent dose up to 0.02 g/50 mL (Fig. 5d). It may be attributed to the increase in availability of surface actives sites on the adsorbent and adsorbent surface area (Garg et al., 2004; Saini et al., 2018). Further increase in adsorbent dose, slight increased in dye removal and finally attained to equilibrium. This observation indicates the overlapping of the surface binding sites with raise in quantity of EDTA@Fe_3O_4/SC ncsdose resulting in decrease in surface active sites and total surface area of adsorbent for cationic dyes adsorption (Ahmed and Ahmaruzzaman, 2015).

3.2.4 Effect of temperature:

The effect of solution temperature on the removal of MB and BG dye was determined in temperature ranges from 27˚C to 57˚C by keeping other experimental condition remains constant. The removal of MB and BG dyes by EDTA@Fe_3O_4/SC increased from 96.7 to 99.8% and 90.0 to 96.0%, respectively with rise in temperature (Fig. 5e). It indicates that MB and BGadsorption process was endothermic in nature (Saini et al., 2018). As temperature increases, the mobility and dispersion of cationic dye molecules in aqueous solution increased which enhance the diffusion of dyes towards external boundary layer followed to internal pores of the adsorbents (Ahmed and Ahmaruzzaman, 2015). It may also attribute the generation of some new surface active sites on the surface of adsorbent for dye adsorption due to the internal bond breakage near the boundary of adsorbents (Rangabhashiyam and Selvaraju, 2015). Similar observation has been reported by other researcher (Bulut and Aydın, 2006; Afroze et al., 2016).

3.2.5 Influence of salinity:

The huge quantities of salts are consumed during dying process in textile industries. It is presumed that it may affect the dye adsorption process also. Therefore, the effect of salinity

on the MB and BG dyes adsorption was carried out by varying the NaCl concentration from 0.05 to 0.8M keeping other adsorption parameters remains constant. The adsorption efficiency of EDTA@Fe_3O_4/SC for MB and BG dyes decreased from 93.0 to 67.3% and 74.8 to 37.7%, respectively with increase in NaCl concentration upto 0.8 M (Fig. 5f). It may be attributed to the screening effect of Na^+ ions and electrically double layer on the surface of adsorbent that reduces the electrostatic attractions between adsorbent and cationic dye molecules (Pimol et al., 2008). The cationic dyes molecules and Na^+ ions in solution struggle for the adsorption on the surface of the adsorbents. Similar observation for dye removal with salinity has been reported by other researchers (Inbaraj and Chen, 2011; Pimol et al., 2008). The concentration of NaCl i.e. 0.6M is equivalent to sea water salinity (3.5%). At this concentration, the adsorption of MB and BG dye was 72.0% and 47.7%, respectively. Finally, it is inferred from the experimental results that presence of salts in water waste significantly affects the removal of dyes by adsorption process.

3.3 Thermodynamic studies:

Thermodynamicswere performed to explore the influence of temperature on the MB and BG dye adsorption onto EDTA@Fe_3O_4/SC. In this study, Gibb's free energy (ΔG^o), entropy (ΔS^o) and enthalpy (ΔH^o) have been calculated. The values of ΔS^o and ΔH^o were calculated from intercept and slope, respectively using linear plots of $\ln K_d$ vs 1/T. The values of these parameters are given in Table 1. The negative value of ΔG^o for both dyes increased with temperature indicates the adsorption process is spontaneous and feasible. The value of ΔH^o for MB dye (75.16 KJ $mole^{-1}$) and BG dye (25.32 KJ $mole^{-1}$) was positive indicates adsorption of cationic dye is endothermic. The positive values of ΔS^o for MB (275.23 J $mol^{-1}K^{-1}$) and BG (102.3 J $mol^{-1}K^{-1}$) dye indicates the high affinity of dye molecules towards adsorbent surface due to erise in randomness and mobility of the system. The high value of ΔS^o and ΔH^o indicates the chemisorption of dye molecules. Cationic dyes molecules chemically bind with surface active sites (X-COO^-) of EDTA@Fe_3O_4/SC (Nandi et al., 2009).

3.4 Adsorption isotherms:

The interaction of dye molecules with adsorbent in solid/liquid interface can be justified by adsorption isotherms modelling. Isotherm models have been employed to experimental data of dye adsorption at various dye concentrations (10-100 mg/L). Four

isotherms models, viz., Langmuir, Freundlich, Temkin and Dubinin- Radushkevich (D-R) model were applied to experimental data. Langmuir model assumes that the monolayer distribution of dye molecules onto the adsorbent surface with fixed number of equivalent active binding sites. There is no communication between adsorbed dye molecules (Langmuir, 1916). Freundlich model is an empirical equation it assumes the multilayer adsorption/distribution of dye molecules onto heterogeneous surface with infinite no. of active sites (Freundlich, 1906). Temkin model assumes the amount of heat energy of adsorbate decrease linearly with monolayer coverage. There is uniform arrangement of active binding sites on the surface (Temkin & Pyzhev, 1940). Dubinin- Radushkevich (D-R) isotherm model is a semi-empirical equation described the adsorption mechanism in solids follows micropore fill. It assumes that the adsorption of molecules onto the heterogeneous surface with Van der Waals forces and is significant for physical sorption process. It indicates the mean free energy and characteristics of adsorbents (Dubinin and Radushkevich, 1947; Boparai et al., 2011). The linear forms of models are described above in section 2.5. The linear plots of different models are given in Fig. 6a-d.

The isotherms model parameters and regression coefficient of each model were calculated using their corresponded linear plots and results summarized in Table 2. The applicability of each model in dyes adsorption experiments was identified by their regression coefficient and isotherms parameters. A comparison of the results showed that Freundlich model was best fitted to MB and BG dyes adsorption process. It indicates the multilayer adsorption of MB and BG dye molecules on the heterogeneous surface active sites. The regression coefficient (R^2) of Freundlich model was found 0.994 and 0.998 for MB and BG dye, respectively. The value of 1/n (slope) was lie in between 0 to 1 i.e., 0.355 for MB and 0.585 for BG indicates that adsorption was favourable and dye molecules chemically bind with the surface of adsorbent.chemisorptions. The value of 1/n below 1 for both dyes designates to chemisorptions on heterogeneous surface of adsorbents. The R_L values of MB and BG dye were found in range 0.068 to 0.422 and 0.012 to 0.109 ($0< R_L>1$) confirmed adsorption process is favourable. The maximum monolayer adsorption capacity ($q_{max.}$) of MB and BG dye was found 227.37mg/g and 285.71mg/g, respectively. It was higher than other reported adsorbents summarized in Table 3. Therefore, the isotherms models studies confirmed that chemisorptions of dye molecules onto EDTA@Fe_3O_4/SC. The lowest value of regression coefficient ($R^2 < 0.850$) of D-R model indicated that dyes molecules adsorbed with the surface functional group of adsorbent by chemical bonding.

3.5 Kinetic modelling:

Kinetic study of MB and BG dyes adsorption was performed to evaluate rate mechanism of adsorption. The adsorption rate of cationic dyes mainly depends upon physico-chemical properties of the adsorbent as well as the process of dye molecules diffusion. In this study, pseudo-first order, pseudo-second order and intraparticle diffusion models were employed to adsorption data of contact time experiments. Pseudo first-order model assumes the rate of dye molecules adsorption with contact time is proportional to the difference in equilibrium cationic dye concentration and quantity of solute adsorbed with time. Mostly, the adsorption initiate by diffusion mechanism through boundary, it follows pseudo-first order rate mechanism (Nandi et al., 2009). Pseudo-second order model assumes the rate determining step of dye adsorption is influenced by chemisorption process. Kinetics models parameters and regression coefficient of each model was calculated from their corresponding linear plots including log ($q_e - q_t$) vs t and t/q_t vs t are given in Fig. 7a-d.The parameter values are summarized in Table 4. Based on the model outputs, it has been inferred that pseudo-second order model is best suited to experimental data. The regression coefficient (R^2) of both dyes was ≥ 0.999 higher than other studied models. The calculated adsorption capacity ($q_{cal.}$) of for both MB and BG dye is similar to the experimental adsorption capacity ($q_{exp.}$). This observation suggested that the rate mechanism of dye adsorption is determined by chemical processes. The cationic dye molecules are electrostatically attracted towards the surface active binding sites (carboxylic and amino groups) of the adsorbents, resulting into chemisorption.

3.6 Intra-particle diffusion model:

This model assumes that the rate mechanism of dye adsorption onto adsorbent occurring in multistage process: i) bulk diffusion, ii) film diffusion, iii) intraparticle or pore diffusion and iv) adsorption through chemical reactions or complexations/ chelation or ion-exhange (Kataria and Garg, 2018). The adsorption of dye molecules depend upon the surface properties and texture of adsorbents (Liu et al., 2013). It is a mass distribution or diffusion process where rate is proportional to square root of time (t). Intraparticle diffusion model parameters were calculated from the plots of q_t vs $t^{1/2}$ (Fig. 7e and f). The plots didn't pass through the origin and high value of boundary layer indicated the intraparticle is not only rate determining steps. It was observed that the dye adsorption occurred as two stages. Initially, the first linear curve indicated the dye molecules rapidly transported from bulk to external

boundary layer of adsorbent via boundary layer or bulk diffusion. Finally, slow linear curve confirmed that the dye adsorption takes place via pore diffusion and chemical bonding on the surface active sites of adsorption. The boundary layer thickness increased with increase in dye concentration which indicates that the adsorption rate of dye molecules controlled by boundary layer diffusion as well as intraparticle diffusion (Rehman et al., 2013). The regression coefficient (R^2) of intraparticle diffusion model for MB and BG dye was less than pseudo-second order model (Table 4). It was inferred that the cationic dyes adsorption on the surface adsorbent (X-COO^-) controlled by chemical process (Liu et al., 2013).

3.7 Dye adsorption in real water sample:

The performance of EDTA@Fe_3O_4/SC nanocomposites for cationic dye removal was studied in water samples of different water sources like canal, tube well, tap water, pond and double distilled water. Adsorption experiment was performed by adding 0.5g of adsorbent in 10mg/L dye concentrations which was prepared using different water samples. It was noticed that the removal efficiency of EDTA@Fe_3O_4/SC nanocomposites for cationic dyes was slightly lower in real water sample as compared to the double distilled water (Fig. 8). It may be due to the presence of other common competitive cationic species like Na^+, Ca^{2+}, Mg^{2+}, Zn^{2+}, $Fe^{3+}$and K^+ in real water sample.

3.8 Cationic dye adsorption mechanism:

Cationic dyes adsorption depends on several process parameters, viz., pHpzc, pH of the solution, surface functional groups, porosity of adsorbents, and nature of dyes also take in account to explore the adsorption mechanism (Zbair et al., 2018; Kataria and Garg, 2018b). Cationic dyes adsorbe onto EDTA@Fe_3O_4/SC through solid/liquid phase interaction; it may be electrostatic interaction, hydrogen bonding, π-π interaction and pore diffusion mechanism (Xu et al., 2013; Gupta et al., 2013; Tran et al., 2017). MB and BG dyes were adsorbed onto adsorbent as following interaction and mechanism:

- Cationic dyes molecules are electrostatic attracted towards the negatively charged EDTA@Fe_3O_4/SC nanocomposites. At pH > pH(pzc), the surface of adsorbent covered with negative charged carboxyl (-COO^-)and Hydroxyl (OH^-) groups which electrically bound or interacted with positively charged (N^+ and S^+ atoms) group of cationic dye molecules. The possible schemes of dye adsorption are given in Fig.9. This electrostatic

interaction made stronger bond between them. Similar observation was reported by Saini et al., (2018) for methylene blue dye at higher pH.

- Cationic dye molecules adsorption onto adsorbent also governed by π-π interaction. EDTA@Fe_3O_4/SC is carbonaceous materials contains organic aromatic structure with C=C bond π-system which interacted with π- electron of aromatic ring of MB and BG dye by π-π interaction. This π-π bonding between dye and adsorbent is slightly weaker than electrostatic bonding.
- Hydrogen bonding also involved on dye adsorption onto adsorbent. At pH ≤ pHpzc, the carboxyl (–COOH) group and water molecules onto surface of adsorbent may be offered H–atoms to initiate hydrogen bonding with polar N– or S–atom of MB and BG dye (Fig. 9). Hydrogen bonding is contribution is relatively less as compared to electrostatic interaction at basic pH.
- The porous structure of carbonaceous EDTA@Fe_3O_4/SC nanocomposites indicates the possibility of cationic dye molecules adsorbed through pore diffusion or filling as well as physical process also.
- FTIR studies of adsorbent before and after cationic dye adsorption indicates that surface functional groups of adsorbent bound with cationic dyes molecules via electrostatic interaction, hydrogen bonding and π-π interaction between them.

3.9 Desorption and Reusability:

Regeneration and reuse potential of an adsorbent is important for economical and sustainable water treatment practices. An excellent or outstanding adsorbent should not only be good in adsorption efficiency but also be productive in regeneration and reusable process. Desorption efficiency of EDTA@Fe_3O_4/SC for both dyes was evaluated using five different desorbing solutions viz., ethanol, methanol, HCl (0.1M), NaOH (0.1M) and distilled water. The optimised condition for this study was mentioned in details of Fig. 10. The desorption efficiency of adsorbent was 83.6% (methanol), 78.2% (ethanol), 80.0% (0.1M HCl), 56.4% (0.1M NaOH), 16.4% (distilled water) for MB dye and 95.0% (methanol), 97.3% (ethanol), 1.4% (0.1M HCl), 8.7% (0.1M NaOH), 9.6% (distilled water) for BG dye (Fig. 10a). The results indicate that cationic dyes adsorbed on the adsorbent were effectively desorbed by organic solvents (ethanol and methanol) as compared to other desorbing solutions (He et al., 2013). The performance of ethanol and methanol depends upon its polarity. Methanol yielded higher desorption that may be due to its polar nature. Methanol contains highly electronegative hydroxyl group which form hydrogen bonding with cationic dye molecules

through electrostatic interaction. Methanol has properties of elution for both polar and non polar compound. Cationic dye molecules are desorbed from the surface due to high solubility in polar methanol solvent and hydrogen bonding between dye molecules and methanol. Therefore, desorption of cationic dyes (MB and BG) were performed using methanol or ethanol. Similar interpretation has been reported by other researcher (Wang et al., 2014).

After desorption experiment, the reusability of adsorbent was evaluated upto five adsorption–desorption cycles. The adsorption efficiency of adsorbent for MB dye continuously decreased with every adsorption-desorption cycle and remained 64% after 5^{th} cycle. While for BG dye, the adsorption efficiency of adsorbent slightly decreased and remained 80% after 5^{th} cycles (Fig. 10b). Hence, EDTA@Fe_3O_4/SC nanocomposites are proficient adsorbent for dye removal because of their high desorption and reusable performance.

4. Conclusion:

The present study concluded that the EDTA functionalised Fe_3O_4/Sawdust Carbon act as promising adsorbent for cationic dyes (MB and BG) removal from aqueous solution. After EDTA modifications, the adsorption efficiency of Fe_3O_4/SC nanocomposites is enhanced upto 99.7% and 96.7% for MB and BG dye, respectively. Freundlich model is well fitted to the experimental data which indicated the multilayer dye adsorption onto nanocomposites. The maximum adsorption capacity of MB and BG dye was 227.3mg/g and 285.7mg/g, respectively that are higher than other reported adsorbents. The rate of MB and BG dye adsorption is followed by pseudo-second order model. Isothermal and kinetic studies indicated the MB and BG dye molecules adsorbed on the surface of EDTA@Fe_3O_4/SC by chemisorption process via compleaxation or ion-exchange or chelation. Thermodynamic studies indicated the dye adsorption process is spontaneous and feasible. Ethanol and methanol are good desorbing solutions for cationic dyes. EDTA@Fe_3O_4/SC is a reusable adsorbent as its removal efficiency after five cycles was 64% and 85% for MB and BG dyes respectively. Therefore, it is concluded that EDTA@Fe_3O_4/SC is a promising adsorbent for cationic dyes with high adsorption, regeneration and reusable efficiency.

Reference:

Afroze, S., Sen, T. K., Ang, M., Nishioka, H., 2016. Adsorption of methylene blue dye from aqueous solution by novel biomass Eucalyptus sheathiana bark: equilibrium, kinetics, thermodynamics and mechanism. Desalin. Water. Treat. 57 (13), 5858–5878.

Ahmed, M. J. K., Ahmaruzzaman, M., 2015. A facile synthesis of Fe_3O_4–charcoal composite for the sorption of a hazardous dye from aquatic environment. J. Environ. Manag. 163, 163–173.

Ai, L., Zhang, C., Liao, F., Wang, Y., Li, M., Meng, L., Jiang, J., 2011. Removal of methylene blue from aqueous solution with magnetite loaded multi-wall carbon nanotube: Kinetic, isotherm and mechanism analysis. J. Hazard. Mater. 198, 282–290.

Boparai H. K., Joseph, M., O'Carroll, D. M., 2011. Kinetics and thermodynamics of cadmium ion removal by adsorption onto nano zerovalent iron particles. J. Hazard. Mater. 186 (1), 458–465.

Bulut, Y., Aydın, H., 2006. A kinetics and thermodynamics study of methylene blue adsorption on wheat shells. Desalination. 194 (1-3), 259–267.

Calvete, T., Lima, E.C., Cardoso, N.F., Dias, S.L.P., Ribeiro, E.S., 2010. Removal of Brilliant Green Dye from Aqueous Solutions Using Home Made Activated Carbons. Clean - Soil Air Water, 38, 521–532.

Chen, J., Feng, J., Yan, W., 2016. Influence of metal oxides on the adsorption characteristics of PPy/metal oxides for Methylene Blue. J. Colloid. Interface. Sci. 475, 26–35.

Crini, G., Badot, P.M., 2008. Application of chitosan, a natural aminopolysaccharide, for dye removal from aqueous solutions by adsorption processes using batch studies: a review of recent literature. Prog. Polym. Sci. 33 (4), 399-447.

Dubinin, M.M., Radushkevich, L.V., 1947. Equation of the characteristic curve of activated charcoal, Chem. Zentr. 1, 875–890.

Duman, O., Tunç, S., Polat, T.G., Bozoğlan, B.K., 2016. Synthesis of magnetic oxidized multiwalled carbon nanotube-κ-carrageenan-Fe_3O_4 nanocomposite adsorbent and its application in cationic Methylene Blue dye adsorption. Carbohydr. Polym. 147, 79–88.

Foo, K.Y., Hameed, B.H. 2010. Insights into the modeling of adsorption isotherm systems. Chem. Eng. J. 156 (1), 2-10.

Freundlich, H.M.F., 1906. over the adsorption in solution, J. Phys. Chem. 57, 385–471

Garg, V.K., Amita, M., Kumar, R., Gupta, R., 2004. Basic dye (methylene blue) removal from simulated wastewater by adsorption using Indian Rosewood sawdust: a timber industry waste. Dyes. Pigm.63 (3), 243–250.

Gupta, V.K., Kumar, R., Nayak, A., Saleh, T.A., Barakat, M.A., 2013. Adsorptive removal dyes from aqueous solution onto carbon nanotubes: a review. Adv. Colloid. Interface Sci. 193, 24–34.

Gürses, A., Hassani, A., Kıranşan, M., Açışlı, Ö., Karaca, S., 2014. Removal of methylene blue from aqueous solution using by untreated lignite as potential low-cost adsorbent: kinetic, thermodynamic and equilibrium approach. Journal of Water Process Engineering. 2, 10–21.

Gusmão, K.A.G., Gurgel, L.V.A., Melo, T.M.S., Gil, L.F., 2013. Adsorption studies of methylene blue and gentian violet on sugarcane bagasse modified with EDTA dianhydride (EDTAD) in aqueous solutions: kinetic and equilibrium aspects. J. Environ. Manag.118, 135–143.

He, X., Male, K.B., Nesterenko, P.N., Brabazon, D., Paull, B., Luong, J.H., 2013. Adsorption and desorption of methylene blue on porous carbon monoliths and nanocrystalline cellulose. ACS Appl. Mater. Interfaces. 5 (17), 8796–8804.

Ho, Y.S., Mckay, G., 1999. Pseudo-second order model for sorption processes. Process. Biochem. 34, 451–465.

Inbaraj, B.S., Chen, B.H., 2011. Dye adsorption characteristics of magnetite nanoparticles coated with a biopolymer poly (γ-glutamic acid). Bioresour. Technol. 102 (19), 8868-8876.

Jamshidi, M., Ghaedi, M., Dashtian, K., Ghaedi, A.M., Hajati, S., Goudarzi, A., Alipanahpour, E., 2016. Highly efficient simultaneous ultrasonic assisted adsorption of brilliant green and eosin B onto ZnS nanoparticles loaded activated carbon: Artificial neural network modeling and central composite design optimization. Spectrochim. Acta. Mol. Biomol. Spectrosc. 153, 257–267.

Jegadeesan, G., Al-Abed, S. R., Sundaram, V., Choi, H., Scheckel, K. G., Dionysiou, D. D. 2010. Arsenic sorption on TiO2 nanoparticles: Size and crystallinity effects. Water Res. 44(3), 965-973.

Joshi, S., Garg, V.K., Saini, J., Kadirvelu, K., 2018. Removal of Toulidine Blue O Dye from Aqueous Solution by Silica-Iron Oxide Nanoparticles. Materials Focus, 7 (1), 140–146.

Kataria, N., Garg, V.K., 2017. Removal of Congo red and Brilliant green dyes from aqueous solution using flower shaped ZnO nanoparticles. J, Environ. Chem. Eng. 5 (6), 5420–5428.

Kataria, N., Garg, V.K., 2018a. Green synthesis of Fe_3O_4 nanoparticles loaded sawdust carbon for Cadmium (II) removal from water: regeneration and mechanism. Chemosphere. 208, 818–828.

Kataria, N., Garg, V.K., 2018b. Optimization of Pb (II) and Cd (II) adsorption onto ZnO nanoflowers using central composite design: isotherms and kinetics modelling. J. Mol. Liq. 271, 228–239.

Kataria, N., Garg, V.K., Jain, M., Kadirvelu, K., 2016. Preparation, characterization and potential use of flower shaped Zinc oxide nanoparticles (ZON) for the adsorption of Victoria Blue B dye from aqueous solution. Adv. Powder. Technol. 27 (4), 1180–1188.

Kumar, N., Mittal, H., Parashar, V., Ray, S.S., Ngila, J.C., 2016. Efficient removal of rhodamine 6G dye from aqueous solution using nickel sulphide incorporated polyacrylamide grafted gum karaya bionanocomposite hydrogel. RSC Adv. 6 (26), 21929-21939.

Lagergren, S., 1898. About the theory of so-called adsorption of soluble substances, K. Sven. vetensk.akad. handl. 24 (4), 1-39.

Langmuir, I., 1916. The constitution and fundamental properties of solids and liquid. J. Am. Chem. Soc. 38, 2221–2295.

Lee, C. K., Lin, K. S., Wu, C. F., Lyu, M. D., Lo, C. C. 2008. Effects of synthesis temperature on the microstructures and basic dyes adsorption of titanate nanotubes. J. Hazard. Mater. 150(3), 494-503.

Lin, Q., Gao, M., Chang, J., Ma, H., 2016. Adsorption properties of crosslinking carboxymethyl cellulose grafting dimethyldiallylammonium chloride for cationic and anionic dyes. Carbohydr. Polym. 151, 283–294.

Liu, F., Chung, S., Oh, G., Seo, T.S., 2012. Three-Dimensional Graphene Oxide Nanostructure for Fast and Efficient Water-Soluble Dye Removal. ACS Appl. Mater. Interfaces. 4, 922−927.

Liu, R.L., Gao, X.Y., An, L., Ma, J., Zhang, J.F., Zhang, Z.Q., 2015. Fabrication of magnetic carbonaceous solid acids from banana peel for the esterification of oleic acid. RSC Adv. 5 (114), 93858–93866.

Liu, Y., Chen, M., Yongmei, H., 2013. Study on the adsorption of Cu (II) by EDTA functionalized Fe_3O_4 magnetic nano-particles. Chem. Eng. J. 218, 46–54.

Makhado, E., Pandey, S., Nomngongo, P.N., Ramontja, J., 2018. Preparation and characterization of xanthan gum-cl-poly (acrylic acid)/o-MWCNTs hydrogel nanocomposite as highly effective re-usable adsorbent for removal of methylene blue from aqueous solutions. J. Colloid Interface Sci. 513, 700-714.

Makhado, E., Pandey, S., Ramontja, J., 2018a. Microwave assisted synthesis of xanthan gum-cl-poly (acrylic acid) based-reduced graphene oxide hydrogel composite for adsorption of methylene blue and methyl violet from aqueous solution. Int. J. Biol. Macromo. 119, 255-269.

Mane, V.S., Babu, P.V.V., 2011. Studies on the adsorption of Brilliant Green dye from aqueous solution onto low-cost NaOH treated saw dust. Desalination. 273, 321–329.

Mittal, H., Alhassan, S.M., Ray, S.S., 2018. Efficient organic dye removal from wastewater by magnetic carbonaceous adsorbent prepared from corn starch. J. Environ. Chem. Eng. 6 (6), 7119-7131.

Mittal, H., Ballav, N., Mishra, S.B., 2014. Gum ghatti and Fe_3O_4 magnetic nanoparticles based nanocomposites for the effective adsorption of methylene blue from aqueous solution. J. Ind. Eng. Chem. 20 (4), 2184-2192.

Mittal, H., Kumar, V., Ray, S.S., 2016. Adsorption of methyl violet from aqueous solution using gum xanthan/Fe_3O_4 based nanocomposite hydrogel. J. Biol. Macromo. 89, 1-11.

Mittal, H., Ray, S.S., 2016. A study on the adsorption of methylene blue onto gum ghatti/TiO_2 nanoparticles-based hydrogel nanocomposite. J. Biol. Macromo. 88, 66-80.

Nandi, B.K., Goswami, A., Purkait, M.K., 2009. Adsorption characteristics of brilliant green dye on kaolin. J. Hazard. Mater. 161 (1), 387–395.

Pandey, S., 2017. A comprehensive review on recent developments in bentonite-based materials used as adsorbents for wastewater treatment. J. Mol. Liq. 241, 1091-1113.

Pandey, S., Ramontja, J., 2016. Turning to nanotechnology for water pollution control: applications of nanocomposites, Focus Sci. 2, 1–10.

Pimol, P., Khanidtha, M., Prasert, P., 2008. Influence of particle size and salinity on adsorption of basic dyes by agricultural waste: dried Seagrape (Caulerpa lentillifera). J Environ. Sci. 20 (6), 760–768.

Rafatullah, M., Sulaiman, O., Hashim, R., Ahmad, A., 2010. Sorption of methyleneblue on low-cost sorbents: a review. J. Hazard. Mater. 177, 70–80.

Ragupathy, S., Raghu, K., Prabu, P., 2015. Synthesis and characterization of TiO_2 loaded cashew nut shell activated carbon and photocatalytic activity on BG and MB dyes under sunlight radiation. Spectrochim. Acta. A Mol. Biomol. Spectrosc. 138, 314–320.

Rangabhashiyam, S., Selvaraju, N., 2015. Efficacy of unmodified and chemically modified Swietenia mahagoni shells for the removal of hexavalent chromium from simulated wastewater. J. Mol. Liq. 209, 487–497.

Rehman, M.S.U., Munir, M., Ashfaq, M., Rashid, N., Nazar, M.F., Danish, M., Han, J.I., 2013. Adsorption of Brilliant Green dye from aqueous solution onto red clay. Chem. Eng. J. 228, 54–62.

Saini, J., Garg, V.K., Gupta, R.K., 2018. Removal of Methylene Blue from aqueous solution by Fe_3O_4@Ag/SiO_2 nanospheres: Synthesis, characterization and adsorption performance. J. Mol. Liq. 250, 413–422.

Saini, J., Garg, V.K., Gupta, R.K., Kataria, N., 2017. Removal of Orange G and Rhodamine B dyes from aqueous system using hydrothermally synthesized zinc oxide loaded activated carbon (ZnO-AC). J. Environ. Chem. Eng. 5 (1), 884–892.

Sancheti, S.V., Saini, C., Ambati, R., Gogate, P.R., (2018). Synthesis of ultrasound assisted nanostuctured photocatalyst (NiO supported over CeO_2) and its application for photocatalytic as well as sonocatalytic dye degradation. Catal. Today. 300, 50-57.

Taneja, P., Sharma, S., Umar, A., Mehta, S.K., Ibhadon, A.O., Kansal, S.K., 2018. Visible-light driven photocatalytic degradation of brilliant green dye based on cobalt tungstate (CoWO4) nanoparticles. Mater. Chem. Phys. 211, 335-342.

Temkin, M.J., Pyzhev, V., 1940. Recent modifications to Langmuir isotherms. Acta. Physiochim. USSR. 12, 217–222.

Tran, H.N., Wang, Y.F., You, S.J., & Chao, H.P., 2017. Insights into the mechanism of cationic dye adsorption on activated charcoal: the importance of π–π interactions. Process. Saf. Environ. 107, 168–180.

Van't Hoff, J.H., 1884. Etudes de dynamique chimique. F. Muller & Co., Amsterdam.

Wang, P., Cao, M., Wang, C., Ao, Y., Hou, J., Qian, J., 2014. Kinetics and thermodynamics of adsorption of methylene blue by a magnetic graphene-carbon nanotube composite. Appl. Surf. Sci. 290, 116–124.

Weber, W.J., Morris, J.C., 1963. Kinetics of adsorption on carbon from solution. J. Sanitary Eng. Div. Am. Soc. Civ. Eng. 89, 31–60.

Xu, J., Lv, H., Yang, S.T., Luo, J., 2013. Preparation of graphene adsorbents and their applications in water purification. Rev. Inorg. Chem. 33 (2), 139–160.

Yang, Y., Wei, X., Sun, P., Wan, J. 2010. Preparation, characterization and adsorption performance of a novel anionic starch microsphere. Molecules. 15(4), 2872-2885.

Yu, X., Wei, C., Wu, H. 2015. Effect of molecular structure on the adsorption behavior of cationic dyes onto natural vermiculite. Sep. Purif. Technol. 156, 489-495.

Zaharia, C. Suteu, D. Muresan, A. Muresan, R., Popescu, A., 2009. Textile wastewater treatment by homogenous oxidation with hydrogen peroxide. Environ. Eng. Manage J. 8 (6), 1359–1369.

Zbair, M., Anfar, Z., Ahsaine, H.A., El Alem, N., Ezahri, M., 2018. Acridine orange adsorption by zinc oxide/almond shell activated carbon composite: Operational factors, mechanism and performance optimization using central composite design and surface modeling. J. Environ. Manag. 206, 383–397.

Caption of Figures:

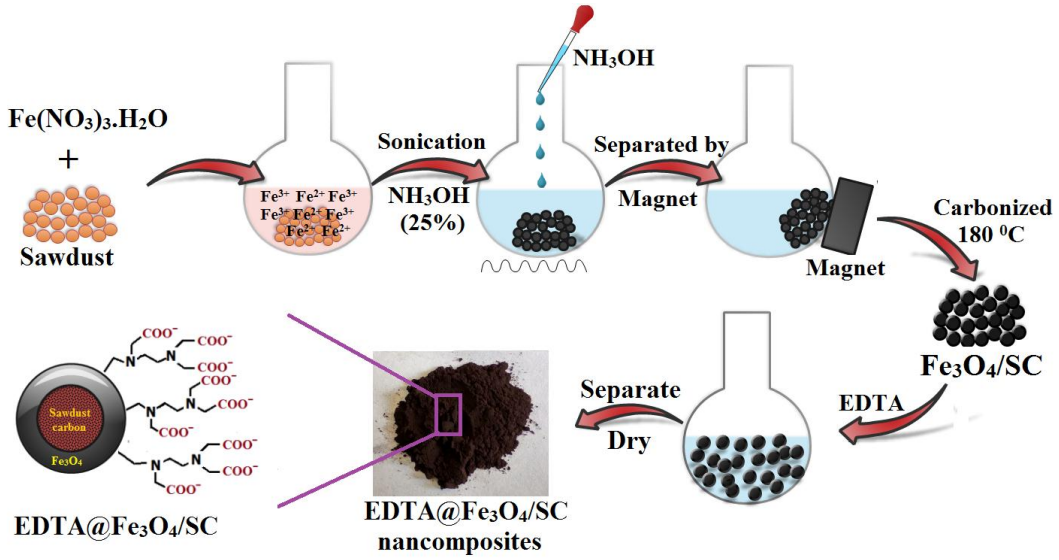

Fig. 1. Schematic description of the preparation of EDTA@Fe_3O_4/SC nanocomposites

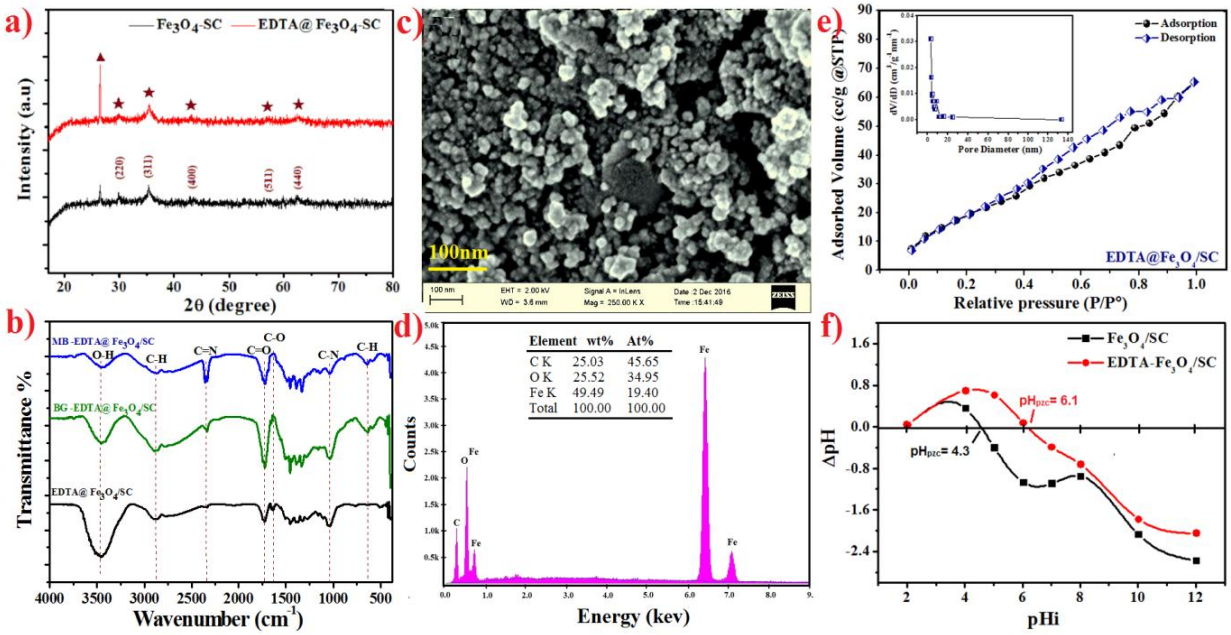

Fig. 2 a) XRD pattern of nanocomposites, b) FTIR spectrum of nanocomposites before and after dye adsorption, c) FESEM image, d) EDX spectra of EDTA@Fe_3O_4/SC e) Nitrogen adsorption–desorption isotherms plot and inset BJH pore size distribution plots and f) Plot between ΔpH versus pHi of nanocomposites.

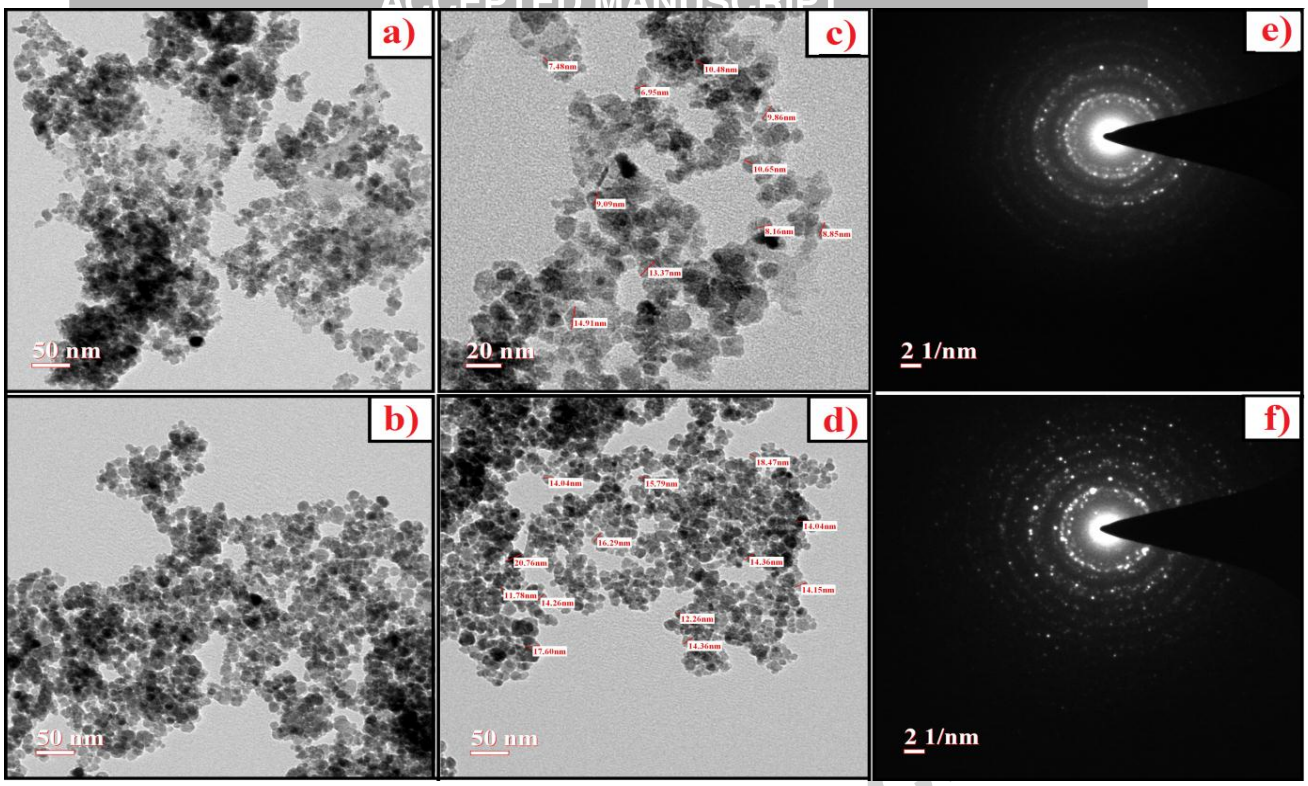

Fig. 3 TEM micrograph of (a and c) Fe_3O_4/SC ncs, (b and d) EDTA@Fe_3O_4-SC ncs and and SAED pattern of e) Fe_3O_4/SC ncs, f) EDTA@Fe_3O_4-SC ncs

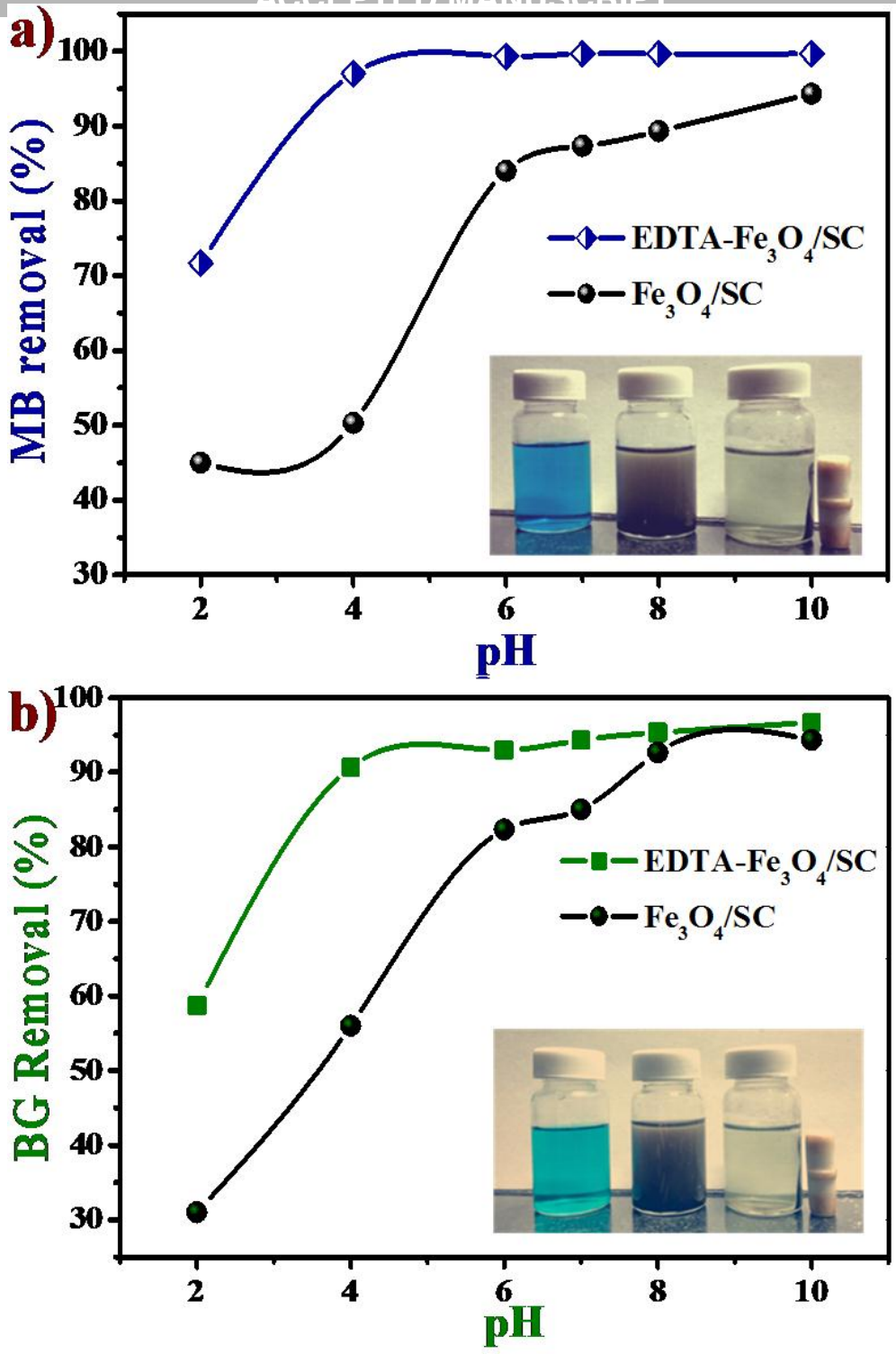

Fig. 4 Effect of pH on a) MB dye and b) BG dye (dye conc. 50 mg/L, temp.- 27 ˚C, adsorbent dose- 0.02g/50mL and time-120 min.)

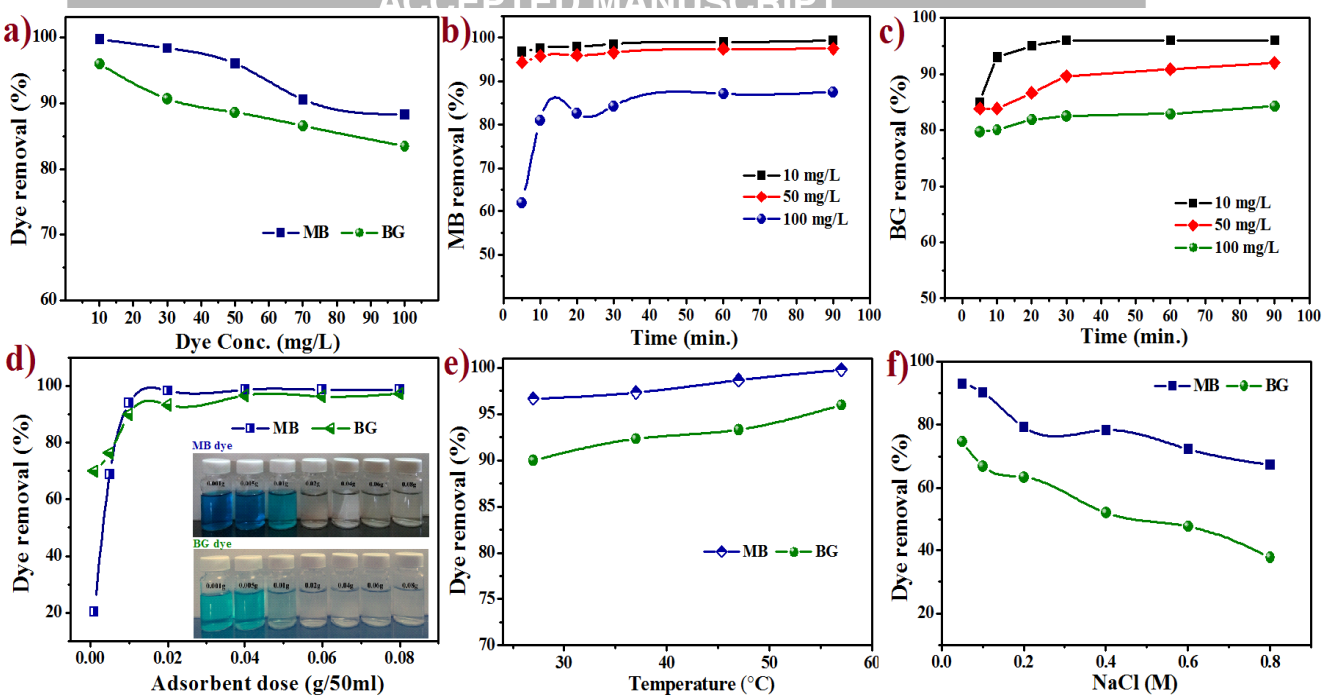

Fig, 5(a) Effect of dye concentration, (b and c) Effect of time on the dye concentration for MB dye and BG dye, d) Effect of adsorbent dose e) Effect of temperature and f) Effect of salinity on removal of MB and BG dye (pH – 6.5, dye conc. 50 mg/L, temp.- 27 ˚C, adsorbent dose- 0.02g/50mL and time-120 min.)

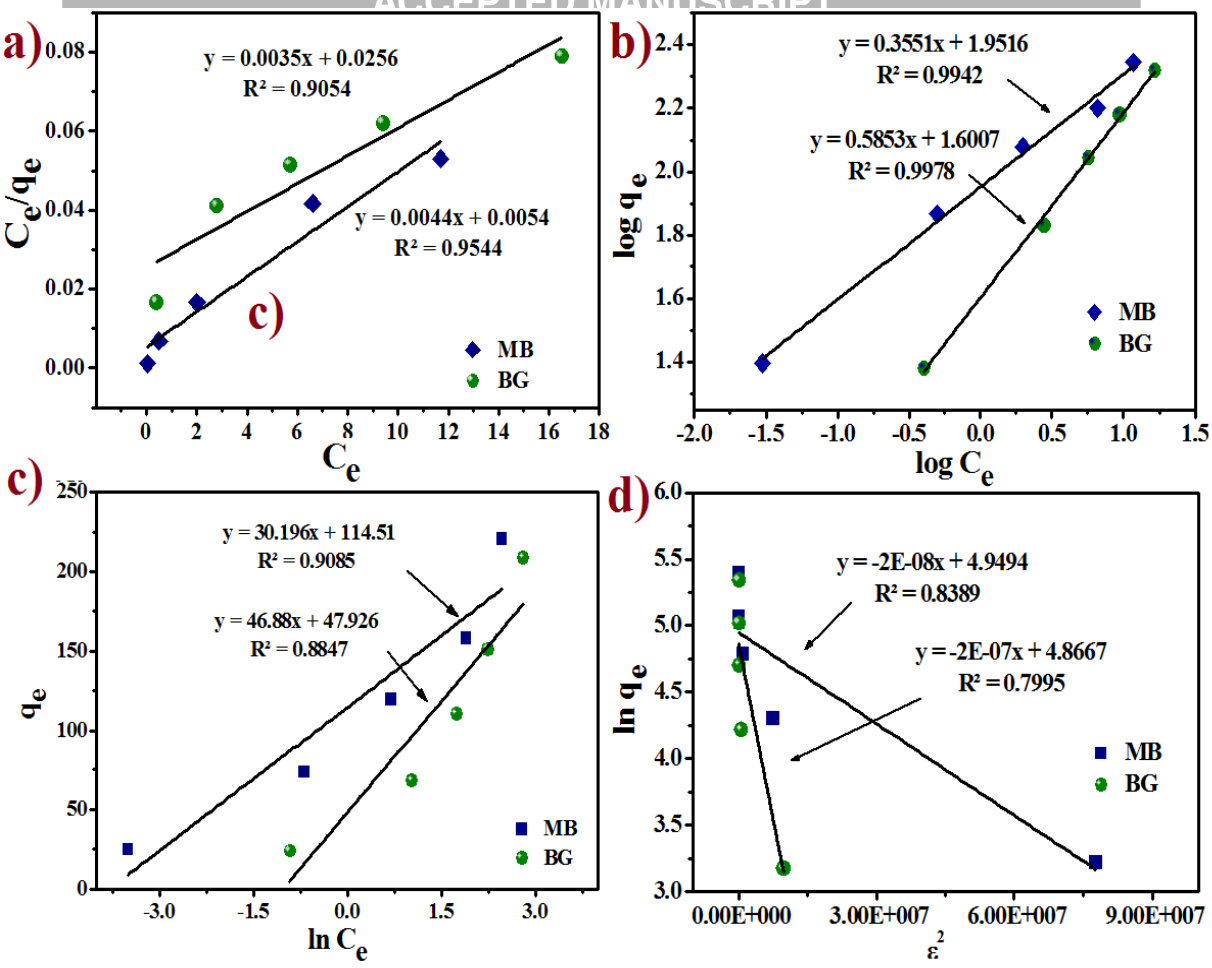

Fig. 6 Isothermal models plots of (a) Langmuir (b) Freundlich (c) Temkin and d) Dubinin-Radushkevich models

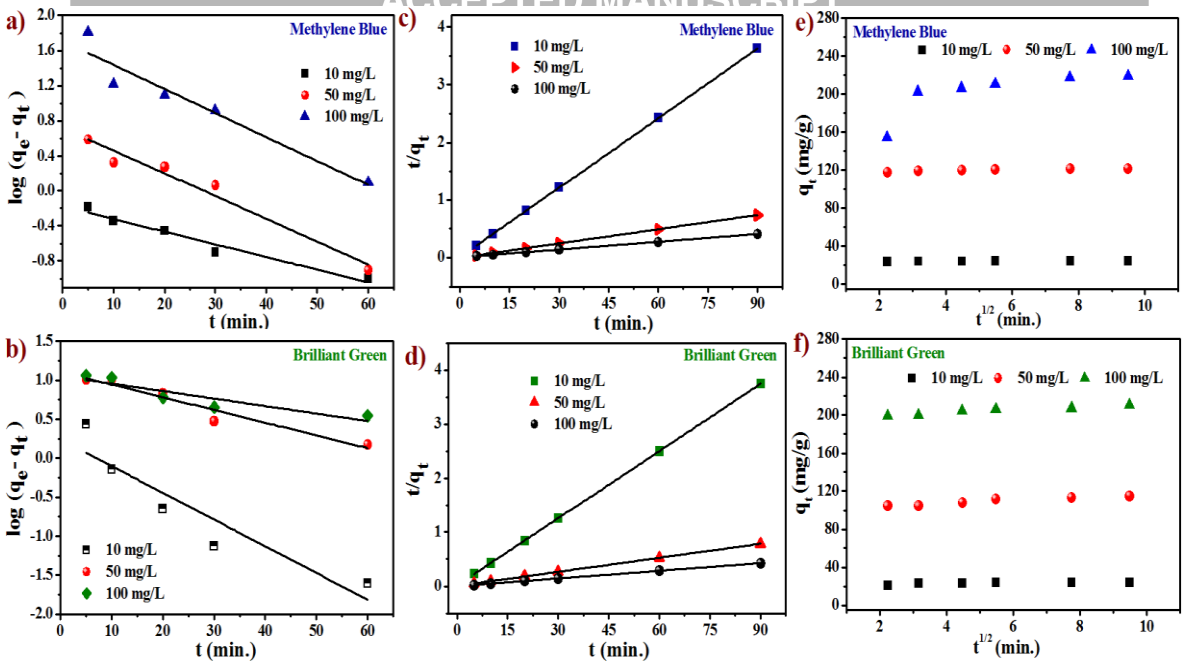

Fig. 7 a,b) Pseudo-first order plot for MB and BG dye removal by EDTA@Fe_3O_4/SC c,d) Pseudo-second order plot for MB and BG dye removal by EDTA@Fe_3O_4/SC and e,f) Intraparticle diffusion plots MB and BG dye removal by EDTA@Fe_3O_4/SC

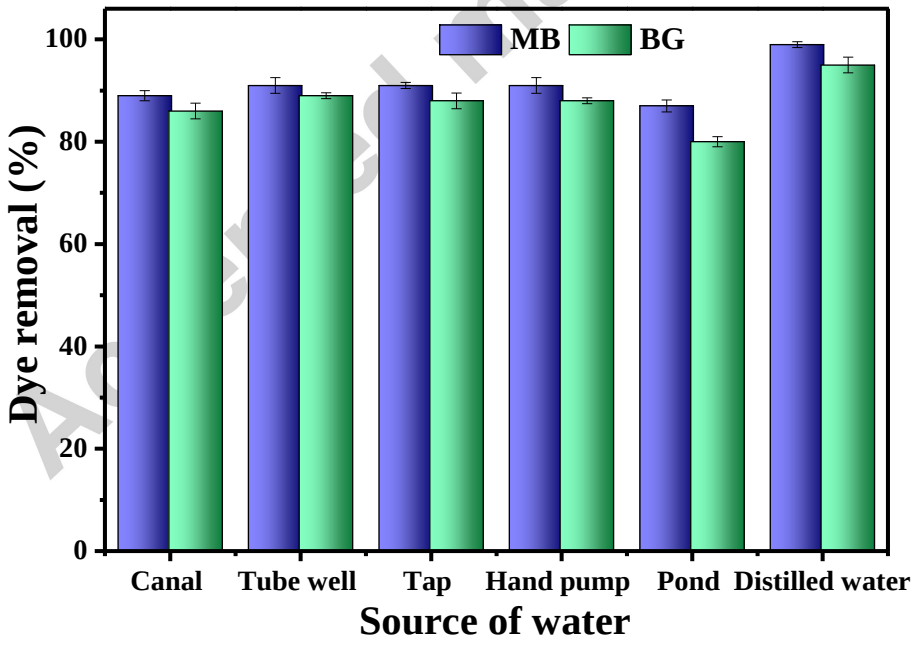

Fig. 8 Removal efficiency of EDTA@Fe_3O_4/SC ncs for MB and BG dye in real water system

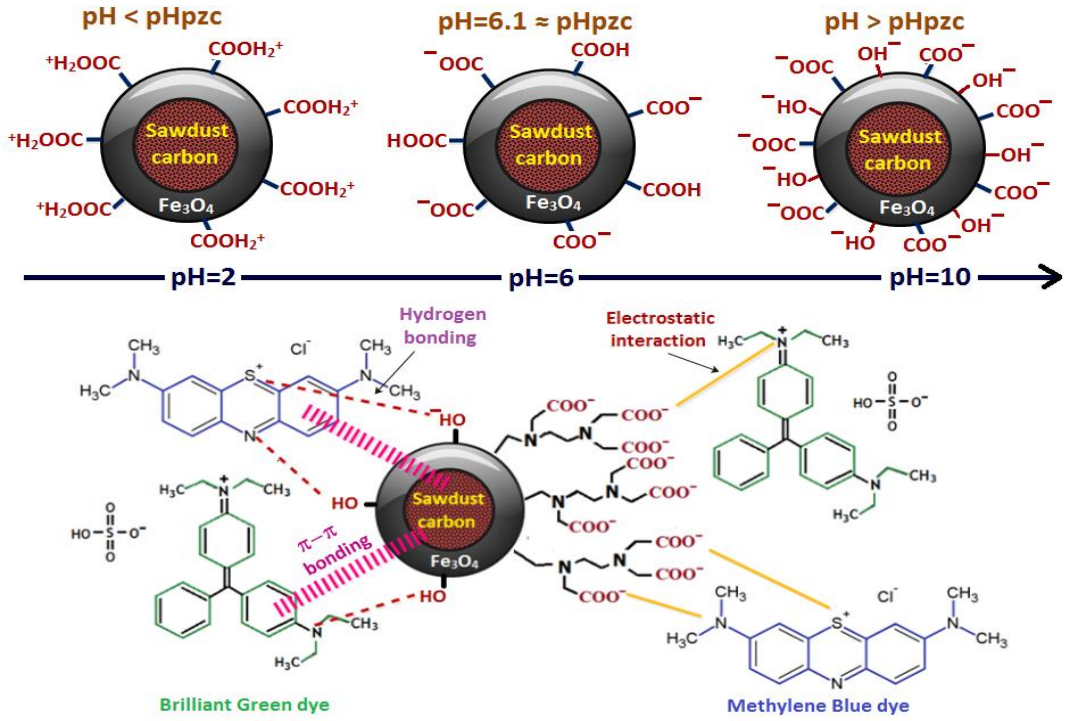

Fig. 9 Possible interaction and mechanism of MB and BG dye adsorption.

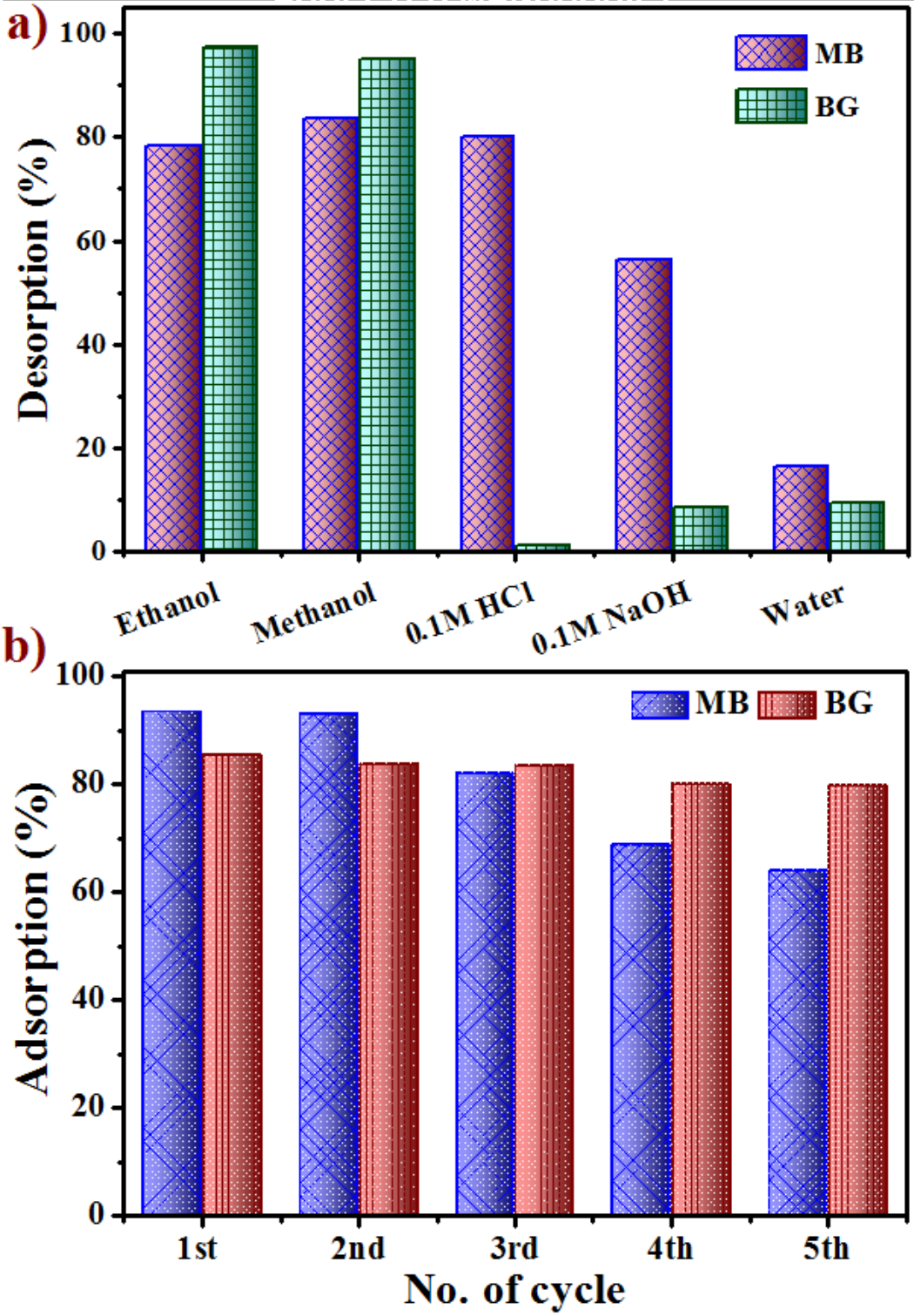

Fig. 10 a) Desorption efficiency of EDTA@Fe_3O_4/SC ncs for MB and BG dye b) Reusability of the EDTA@Fe_3O_4/SC for MB and BG dyes removal (dye conc.-30 mg/L, pH- natural, temp- 27±˚C, dose- 0.02g and time- 120 min.)

Table 1 Thermodynamic parameters description for MB and BG dye adsorption onto the EDTA@Fe_3O_4/SC ncs

Temp.	**Methylene Blue (MB)**			**Brilliant Green (BG)**		
(K)	**ΔG°**	**ΔS°**	**ΔH°**	**ΔG°**	**ΔS°**	**ΔH°**
	(k J mol^{-1})	**(J mol^{-1}K^{-1})**	**(k J mol^{-1})**	**(k J mol^{-1})**	**(J mol^{-1}K^{-1})**	**(k J mol^{-1})**
300	-8.398	275.23	75.16	-5.480	102.30	25.32
310	-9.271			-6.414		
320	-11.450			-7.021		
330	-17.045			-8.719		

Table 2 Adsorption isotherms models parameters for MB and BG dye adsorption on EDTA@Fe_3O_4/SC ncs

Isotherms model	**Parameters**	**Parameters values**	
		MB	**BG**
Langmuir	q_{max} (mg/g)	227.27	285.71
	b (L/mg)	0.815	0.137
	R^2	0.9544	0.9044
Freundlich	1/n	0.355	0.585
	K_f (mg/g)	89.45	39.87
	R^2	0.994	0.998
Temkin	b_T	82.60	53.20
	K_T (L/mg)	44.34	2.78
	R^2	0.909	0.885
Dubinin- Radushkevich	Q_s (mg/g)	141.02	129.83
	K_D (mol^2/KJ^2)	2 x 10^{-8}	2 x 10^{-7}
	E (KJ/mol)	5	1.58
	R^2	0.839	0.800

R_L Values

Initial Dye conc.	**10 mg/L**	**30 mg/L**	**50 mg/L**	**70 mg/L**	**100 mg/L**
MB	0.422	0.196	0.128	0.095	0.068
BG	0.109	0.039	0.024	0.017	0.012

Table 3 Comparison in Adsorption capacity of other reported adsorbents for MB and BG dyes

Adsorbents	**Dyes**	**$q_{max.}$ (mg/g)**	**Reference**
Kaolin	BG	65.4	Nandi et al., 2009
CAC	BG	219	Calvete et al., 2010
CPAC	BG	263	Calvete et al., 2010
NaOH treated saw dust	BG	58	Mane and Babu, 2011
Red clay	BG	125	Rehman et al., 2013
ZnS-NP-AC	BG	142.9	Ghaedi et al., 2015
ZnS-NP-AC	BG	250	Jamshidi et al., 2016
ZnO nps	BG	238.1	Kataria and Garg, 2017
EDTA@Fe_3O_4-SC	BG	285.7	present study
Porous Carbon Monoliths	MB	127.5	He et al., 2013
Magnetic GO-CNTs	MB	65.8	Wang et al., 2014
Magnetic GO	MB	24.9	Wang et al., 2014
Magnetic CNTs	MB	43.9	Wang et al., 2014
Fe_3O_4charcoal composite	MB	97.5	Ahmed and Ahmaruzzaman, 2015
PPy/Fe_3O_4	MB	92.08	Chen et al., 2016
PPy/SiO_2	MB	104.71	Chen et al., 2016
PPy/Al_2O_3	MB	134.77	Chen et al., 2016
Fe_3O_4@Ag/SiO_2	MB	128.1	Saini et al., 2018
EDTA@Fe_3O_4-SC	MB	227.3	present study

Table 4 Kinetic models parameters for MB and BG dye adsorption on EDTA@Fe_3O_4/SC ncs.

Kinetics	**Parameters**	**Methylene Blue**			**Brilliant Green**		
		10 mg/L	**50 mg/L**	**100 mg/L**	**10 mg/L**	**50 mg/L**	**100 mg/L**
Pseudo-first order	k_1	0.0041	0.060	0.063	0.079	0.038	0.022
	q_e (cal)	1.51	5.29	51.33	1.74	12.83	11.32

	R^2	0.965	0.969	0.929	0.869	0.946	0.844
Pseudo-second order	k_2	0.167	0.031	0.003	0.100	0.008	0.008
	q_e (cal)	24.88	121.9	222.2	24.07	116.3	212.8
	R^2	0.999	0.999	0.999	0.999	0.999	0.999
Intraparticle diffusion	k_{id}	0.084	0.494	6.600	0.276	1.545	1.537
	C	24.10	117.7	166.0	21.85	101.3	196.4
	R^2	0.931	0.877	0.579	0.514	0.9187	0.925
Exp. data	q_e (exp)	24.9	121.9	219.2	24.3	115.2	210.8

Highlights:

- EDTA@Fe_3O_4/SC nanocomposites were synthesized by low cost green synthesis approach.
- Adsorption capacity EDTA@Fe_3O_4/SC nanocomposites for MB and BG dyes were 227 mg/g and 285 mg/g, respectively.
- Reusable and desorption potential of EDTA@Fe_3O_4/SC nanocomposites was explored.
- Freundlich and pseudo second order model is best fitted in dye adsorption.
- Application of EDTA@Fe_3O_4/SC nanocomposites in natural water was also evaluated.